Geophysical Research Letters

RESEARCH LETTER
10.1029/2024GL111083

Seasonal Upwelling Forecasts in the California Current System

Dillon J. Amaya[1], Michael G. Jacox[1,2], Michael A. Alexander[1], Steven J. Bograd[2,3], and Liwei Jia[4]

[1]Physical Sciences Laboratory, NOAA, Boulder, CO, USA, [2]Southwest Fisheries Science Center, NOAA, Monterey, CA, USA, [3]Department of Ocean Sciences, University of California-Santa Cruz, Santa Cruz, CA, USA, [4]Geophysical Fluid Dynamics Laboratory, NOAA, Princeton, NJ, USA

Key Points:

- Global climate models skillfully predict upwelling in the California Current System in winter-summer
- Models also skillfully predict timing of spring transition
- Winter skill is linked to the El Niño-Southern Oscillation and North Pacific Oscillation, summer skill with the Pacific Meridional Mode

Supporting Information:

Supporting Information may be found in the online version of this article.

Correspondence to:

D. J. Amaya,
dillon.amaya@noaa.gov

Citation:

Amaya, D. J., Jacox, M. G., Alexander, M. A., Bograd, S. J., & Jia, L. (2024). Seasonal upwelling forecasts in the California Current System. *Geophysical Research Letters*, *51*, e2024GL111083. https://doi.org/10.1029/2024GL111083

Received 9 JUL 2024
Accepted 8 NOV 2024

Author Contributions:

Conceptualization: Dillon J. Amaya, Michael G. Jacox, Michael A. Alexander, Steven J. Bograd
Data curation: Dillon J. Amaya, Michael G. Jacox, Liwei Jia
Formal analysis: Dillon J. Amaya
Investigation: Dillon J. Amaya
Methodology: Dillon J. Amaya, Michael G. Jacox
Project administration: Dillon J. Amaya
Resources: Dillon J. Amaya
Software: Dillon J. Amaya

Abstract Coastal upwelling plays a vital role in the support and maintenance of productive marine ecosystems throughout the California Current System (CCS). Here, we evaluate upwelling forecast skill using ~30 years of seasonal reforecasts from four global climate models contributing to the North American Mulitmodel Ensemble (NMME). The models skillfully predict upwelling intensity throughout much of the CCS in boreal winter, and in the South-Central CCS in spring/summer. The models also skillfully predict various aspects of upwelling phenology, including the timing of the spring transition, as well as the total vertical transport integrated over the course of the upwelling season. Climatic sources of forecast skill vary with season, with contributions from the El Niño-Southern Oscillation in winter-spring, and the North Pacific Oscillation and the North Pacific Meridional Mode in the winter-summer. Our results highlight the potential of seasonal climate forecasts to inform management of upwelling-sensitive marine resources.

Plain Language Summary Upwelling—the process of drawing cold, nutrient rich ocean waters toward the surface—plays a vital role in supporting vibrant and diverse biological populations throughout the California Current System (CCS). Here, we assess whether four global climate models can forecast seasonal upwelling 1–12 months in advance. We show that for much of the year (winter through summer), models can predict anomalous upwelling intensity several months in advance. We also show that the models can predict the timing of the "spring transition" (i.e., the start of the upwelling season) for much of the CCS. The model skill is related to large-scale climate modes, including the El Niño-Southern Oscillation, the North Pacific Oscillation, and the Pacific Meridional Mode. These climate modes alter the strength of the surface winds along the U.S. west coast from winter-summer, giving rise to predictable patterns of upwelling. Our results highlight the potential of seasonal climate forecasts to inform management of upwelling-sensitive marine resources.

1. Introduction

The increasingly apparent impacts of climate variability and change on sensitive marine ecosystems have led to a growing desire among marine resource managers to fold forward-looking environmental information into their decision-making strategies (Cannizzo & Selz, 2021; Tommasi et al., 2017). Consequently, there has been a concerted effort to develop, evaluate, and maintain ocean forecasts for marine ecosystem applications, especially on seasonal (1–12 months) timescales (Amaya et al., 2022; Hervieux et al., 2019; Hobday et al., 2018; Jacox et al., 2020, 2022, 2023; Payne et al., 2017; Siedlecki et al., 2016; Stock et al., 2015; Tommasi et al., 2017). While there has been substantial progress in ocean forecasting, bottlenecks associated with climate model resolution and the availability of oceanographic output still exist (Minobe et al., 2022). For example, most modeling centers typically only save surface variables such as sea surface temperature (SST) or sea surface height (SSH) for analysis. As a result, a thorough forecast skill assessment of other ecologically relevant ocean parameters across a suite of global climate models has proven challenging, although recent studies exploring dynamical downscaling as a method for generating comprehensive ocean forecasts have shown promise (Jacox et al., 2023; Kearney et al., 2021; Siedlecki et al., 2016).

Even with current computational constraints, there is still space for exploration. In particular, one important oceanic process—upwelling—can be estimated from existing atmospheric model output, thereby circumventing many issues of data availability. Wind-driven upwelling plays a vital role in drawing nutrient-rich water from depth, supporting vibrant and diverse biological populations across trophic levels. In particular, wind-driven coastal upwelling in the California Current System (CCS) contributes to disproportionately high primary

Supervision: Dillon J. Amaya, Michael G. Jacox, Michael A. Alexander, Steven J. Bograd
Validation: Dillon J. Amaya
Visualization: Dillon J. Amaya
Writing – original draft: Dillon J. Amaya
Writing – review & editing: Dillon J. Amaya, Michael G. Jacox, Michael A. Alexander, Steven J. Bograd, Liwei Jia

productivity and fish catch (e.g., Chavez & Messié, 2009), and disruptions to the magnitude or timing of upwelling can have impacts that cascade through the food web (e.g., Barth et al., 2007; Black et al., 2011), as was observed across multiple trophic levels during the delayed spring transition in 2005 (Henson & Thomas, 2007; Schwing et al., 2006). As a result, accurate seasonal upwelling forecasts could inform a variety of key management decisions, such as fish catch limits and the timing of fishery closures (Tommasi et al., 2017).

In this study, we leverage output from four global climate models to evaluate the seasonal forecast skill of wind-driven coastal upwelling in the CCS over the last ∼30 years, with an emphasis on intensity and indicators of phenology (Bograd et al., 2009; Jorgensen et al., 2024). We then explore possible climatic sources of forecast skill for different seasons.

2. Data and Methods

2.1. Wind-Driven Upwelling Reforecasts

Reforecasts (i.e., forecasts of past periods, using information that was only available at the time of initialization) of wind-driven upwelling are derived from daily mean wind stress reforecasts from four global climate models contributing to the North American Multimodel Ensemble (NMME; Becker et al., 2022; Kirtman et al., 2014): the Canadian Earth System Model version 5.0 (CanESM5; Diro et al., 2024; Sospedra-Alfonso et al., 2021), the Canadian Center for Climate Modeling Analysis Coupled Climate Model version 4 (CanCM4i; Lin et al., 2020), the Community Earth System Model version 1 (CESM1; Small et al., 2014), and the Geophysical Fluid Dynamics Laboratory Seamless System for Prediction and Earth System Research (GFDL-SPEAR; Delworth et al., 2020; Lu et al., 2020). Reforecasts span 365 days, initialized on the first of every month from 1991 to 2021. Each model has 1° horizontal resolution except GFDL-SPEAR, which has 0.5° horizontal resolution. Forecasts from CanCM4i and CESM1 consist of 10 members each, while forecasts from GFDL-SPEAR and CanESM5 have 15 and 20 members, respectively.

Coastal upwelling in the CCS is driven primarily by a combination of wind-driven Ekman transport and cross-shore geostrophic flow associated with the alongshore pressure gradient (Jacox et al., 2018). The NMME models did not save the daily mean SSH output needed to calculate the geostrophic term, so we limit our upwelling forecast evaluation to the wind-driven component, which is the dominant of the two (Jacox et al., 2018). Following Ding et al. (2021) and Jacox et al. (2018), we calculate wind-driven Ekman transport (units of $m^2\ s^{-1}$) in the zonal (U_{ek}) and meridional (V_{ek}) directions as:

$$U_{ek} = \frac{\tau_y}{\rho f};\ V_{ek} = \frac{-\tau_x}{\rho f} \tag{1}$$

where τ_x and τ_y are the zonal and meridional surface wind stress respectively, ρ is a reference density for seawater (assumed here to equal 1,025 kg m^{-3}), and f is the Coriolis parameter.

To derive forecasts of Ekman-induced upwelling (W_{ek}) we integrate the zonal and meridional Ekman transports around the perimeter of 1° latitudinal regions centered on 31°N–47°N and extending ∼75 km offshore of the US west coast. For the models with 1° grids, we calculate the total volume transport per meter of coastline (i.e., $m^3\ s^{-1}$ per m of coastline or simply $m^2\ s^{-1}$) by summing the Ekman transport components along the faces of the ocean grid cell nearest to land (excluding the sides representing the coastline where transports are zero), and then dividing by the distance along the coast covered by the grid cell. In the higher-resolution GFDL-SPEAR, Ekman transports for each 1° bin were integrated around all ocean grid cells within ∼75 km of the coast. Using this method, the models are generally able to reproduce the observed climatological timing and intensity of the upwelling season at each latitude (Figure S1 in Supporting Information S1). Note that W_{ek} implicitly captures both coastal divergence (due to offshore Ekman transport near the coast) and Ekman pumping/suction (due to wind stress curl); we do not explicitly quantify their individual contributions, which are not spatially separable (Capet et al., 2004).

To assess predictive skill for upwelling intensity, we use the 365-day W_{ek} forecasts to construct and evaluate monthly mean forecasts from 0.5 months (e.g., forecasts of January, initialized at the beginning of January) to 11.5 months (e.g., forecasts of December, initialized at the beginning of January). Monthly mean forecast anomalies are based on a lead-dependent climatology from 1991 to 2021. The lead-dependent climatology (e.g.,

Stock et al., 2015) was calculated by averaging all of the forecasts for each respective initialization month and lead time (e.g., averaging all January initializations at 1.5-month lead). This average was then subtracted from the lead-dependent forecasts to generate anomalies. Removing a lead-dependent climatology essentially bias-corrects the models as they drift from the observed initialized state to their preferred model state. Forecasted anomalies are also smoothed with a 3-month running mean prior to analysis. To assess predictive skill for upwelling phenology (next section), daily resolution is retained.

2.2. Upwelling Phenology

We further evaluate forecasts of various metrics of upwelling phenology (i.e., changes in the amplitude and phasing of seasonal events (Bograd et al., 2009; Jorgensen et al., 2024)). The phenology metrics are based on the Cumulative Upwelling Index (CUI) at each latitude, which is the cumulative sum of the total daily mean W_{ek} starting on January 1 through the end of the year. From CUI, we define the Spring Transition Index (STI) as the Julian day each year in which the CUI reaches its minimum value (i.e., the date after which the integrated effects of upwelling dominate over downwelling, thus marking the beginning of the upwelling season). Similarly, we define the end of the upwelling season (END) as the Julian day each year when the CUI reaches its maximum value. Finally, we calculate the Total Upwelling Magnitude Index (TUMI), which is the total integrated W_{ek} from STI to END. STI, END, and TUMI each have one value per year. We remove the 1991–2021 mean from each metric to calculate anomalies.

Forecasted CUI is based on the January initializations from each model, and is calculated for each ensemble member separately and for the length of the 365-day forecast. We then calculate STI, END, and TUMI for each ensemble member before taking the ensemble mean to assess skill. The multi-model mean (MMM) phenology forecasts are taken as the average of the 55 phenology forecasts from all ensemble members across all models.

2.3. Verification Data Set and Skill Metrics

Forecasts are verified against the daily/monthly mean W_{ek} from the National Oceanic and Atmospheric Administration (NOAA) operational upwelling indices (Jacox et al., 2018), which are based on historical and near-real-time CCS reanalyses (CCSRA) developed by the Ocean Modeling group at the University of California Santa Cruz (Neveu et al., 2016; oceanmodeling.ucsc.edu). Note that NOAA's W_{ek} is identical to the Ekman component of the Coastal Upwelling Transport Index (CUTI; Jacox et al., 2018), but without the geostrophic component. The CCS reanalyses use the Regional Ocean Modeling System (ROMS) with 0.1° horizontal resolution and span a region encompassing the CCS from 30°N–48°N, extending offshore to 134°W. The atmospheric forcing data for ROMS varies over the length of the run as the reanalysis transitions from the historical to near-real time components. Full details on the different atmospheric forcing data can be found in Section 4.1 of Jacox et al. (2018). See also Neveu et al. (2016) and Amaya et al. (2023) for additional model details.

Deterministic forecast skill is based on anomaly correlation coefficient (ACC), where significance is calculated using a 95% confidence interval based on a two-sided *t*-test. We further compare the model forecast skill to persistence forecasts that are generated by propagating CCSRA W_{ek} anomalies from the month preceding the forecast initialization for the length of the forecast (i.e., 12-month). We also assess the quality of probabilistic forecasts of each phenology metric in upper and lower terciles (e.g., forecasted chances of having a late or early STI) using the Brier Skill Score (BSS), which represents the mean square error of the probabilistic forecast (known as the Brier Score; *BrS*) relative to the skill of a reference forecast (BrS_{ref}).

$$BrS = \frac{1}{N}\sum_{i=1}^{N}\left(f_i - o_i\right)^2 \tag{2}$$

$$BSS = 1 - BrS/BrS_{ref} \tag{3}$$

$$BrS_{ref} = \frac{1}{N}\sum_{i=1}^{N}\left(\overline{o} - o_i\right)^2 \tag{4}$$

where N is the total number of forecasts being evaluated (for phenology forecasts, $N = 31$), f_i is the forecast probability of falling within a target tercile (e.g., the fraction of ensemble members in the upper/lower tercile) for

a given initialization i, and o_i is the observed probability (i.e., either 1 or 0). The BSS ranges from negative infinity (no skill) to 1 (perfect skill), with scores above 0 indicating forecasts that are better than random chance.

The BrS_{ref} is typically calculated for the climatological likelihood ($\overline{o}$) of observations falling within a tercile or 33%; however, $\overline{o}$ for STI and END is not 33% at every latitude. For example, due to near year-round upwelling, the observed STI (END) consistently falls within the first (last) three weeks of the year from 31°N-34°N (Figure S2 in Supporting Information S1). As a result, the lower terciles of the observed STI distribution at these latitudes are all equal to the earliest possible STI date (i.e., January 1), which prevents any data from falling below the lower tercile and leads to $BrS_{ref} = \overline{o} = o_i = 0$ and BSS being undefined (Figure S3 in Supporting Information S1). The END term has a similar issue with the upper tercile being equal to the latest possible END date (i.e., December 31). Therefore, at latitudes with consistent upwelling, STI and END may be less physically meaningful than at higher latitudes with more well-defined upwelling and downwelling seasons.

To account for this potential issue, we limit our forecast evaluation of STI/END to latitudes that have large observed year-to-year variability such that these terms are more evenly distributed. This is done by calculating BrS_{ref} for both STI and END at each latitude and tercile separately, and then masking the STI (END) forecasts at each latitude where $BrS_{ref} = 0$ for lower (upper) tercile. Note that we do not apply these masks during our BSS skill evaluation of upper (lower) tercile STI (END) forecasts since $BrS_{ref} \neq 0$, though $\overline{o}$ may not equal 0.33 (Figure S3 in Supporting Information S1). In these instances, the BSS represents the forecast skill of predicting STI (END) values in the upper (lower) Xth percentile, where X is 100 times $\overline{o}$ at that latitude.

2.4. Other Climate Data and Indices

In Section 3.3, we explore climatic sources of upwelling forecast skill using monthly mean SST data from the NOAA Optimum Interpolation SST version 2.1 (OISST; Huang et al., 2021) and monthly mean sea level pressure (SLP) data from the ERA5 reanalysis (Hersbach et al., 2020) from 1991 to 2021. Monthly mean SST and SLP anomalies (SSTA and SLPA, respectively) are calculated relative to a climatological period of 1991–2021, are subject to a 3-month running mean, and have a linear trend removed at each grid cell. Regression maps of SSTAs and SLPAs are generated by calculating the slope of the linear least squares fit between their anomalies at each grid cell and principal component (PC) timeseries describing the leading modes of W_{ek} variability.

We further compare W_{ek} anomalies to variability associated with three climate modes—the El Niño-Southern Oscillation (ENSO), the North Pacific Oscillation (NPO), and the North Pacific Meridional Mode (PMM). ENSO variability is estimated using the Nino3.4 index (SSTAs averaged 5°S–5°N, 170°W–120°W), while PMM variability is estimated with the PMM SST index available at https://psl.noaa.gov/data/timeseries/monthly/PMM/ (Chiang & Vimont, 2004). The NPO index is taken to be the 2nd empirical orthogonal function (EOF) of 3-month running mean SLPAs from ERA5 in the North Pacific from 30°N–65°N.

3. Results

3.1. Forecast Skill of Upwelling Intensity

Monthly mean W_{ek} forecasts of boreal winter/early spring from CanESM5, CanCM4i, and GFDL-SPEAR have significant skill in the North CCS (41°N–47°N) (Figure 1). This seasonally enhanced skill is less apparent in CESM1, although it is a major feature of the MMM forecasts and extends to 9.5-month lead when forecasting January to March. The elevated skill in winter is likely associated with ENSO teleconnections (e.g., Jacox et al., 2019), which tend to give rise to more deterministic and skillful forecasts. While this "ENSO band" of increased skill is most apparent in the North CCS, a similar feature can be seen in the MMM forecasts in Central CCS (35°N–40°N) and, to a lesser extent, in the South CCS (31°N–35°N), consistent with previous studies of CCS SST forecasts (Jacox et al., 2019).

There is another period of significant forecast skill in the Central CCS for forecasts of boreal spring and summer (Figure 1 middle row). This "warm season band" of increased skill is most coherent in CanCM4i and CESM1, and extends to about 7.5-month lead in the MMM when forecasting May-August. It is also seen in the South CCS, with significant skill in the MMM out to 5.5-month lead when forecasting April-May. The long-lead skill in summer is surprising given the lack of persistence-based skill and that ENSO teleconnections tend to be strongest

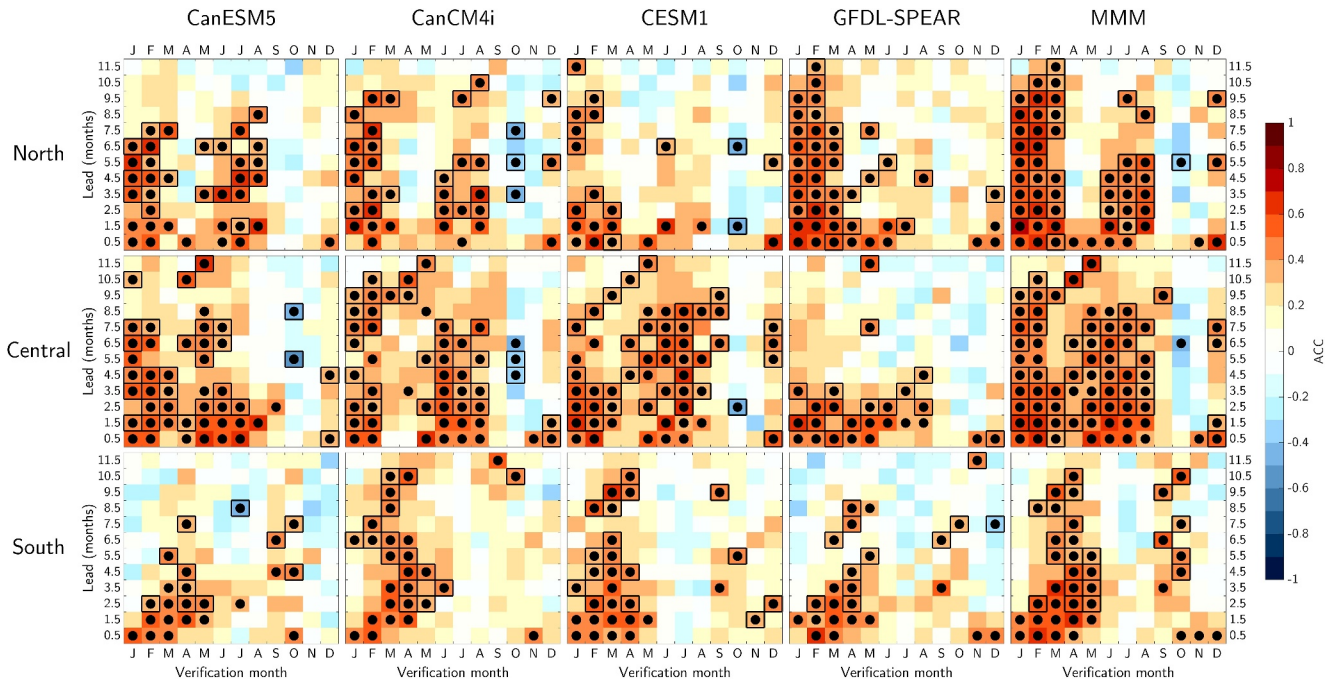

Figure 1. Monthly mean upwelling forecast skill (based on ACC) for each model and the MMM (columns) in three different CCS regions (rows). Skill is a function of verification month (*x*-axis) and lead time (*y*-axis). Black circles indicate ACC values significantly greater than 0 with 95% confidence. Black boxes indicate ACC values significantly greater than 0 when persistence forecast skill is not significantly greater than 0.

in winter. This suggests that there may be other climatic sources of upwelling forecast skill independent of ENSO. We will explore this possibility in Section 3.3.

3.2. Forecast Skill of Upwelling Phenology

January initialized forecasts show significant skill when predicting the STI in the Central CCS from 38°N–0°N, with CanESM5, CESM1, and GFDL-SPEAR exhibiting the highest ACCs (Figure 2a). In contrast, none of the models have consistent skill when predicting END, except for GFDL-SPEAR at 42°N and 46°N–47°N (Figure 2b). The models may be able to predict STI better than END for several reasons. First, for January initialized forecasts, STI occurs earlier than END (i.e., at shorter lead times), and may benefit from memory of the initial condition (though note that END forecasts based on July initializations also have poor skill; Figure S4 in Supporting Information S1). Second, forecast skill of W_{ek} intensity is weakest when forecasting fall (Figure 1), indicating that upwelling in this season is less predictable overall, regardless of when forecasts are initialized.

Forecasts from CanESM5, CanCM4i, and CESM1 skillfully predict TUMI in the Central CCS from 35°N–38°N, with the region of significant skill in CESM1 extending to 43°N (Figure 2c). In contrast, GFDL-SPEAR shows significant TUMI skill for more isolated regions, including 31°N–32°N, 35°N, 37°N, and 41°N–42°N. The MMM TUMI forecasts have significant skill from 31 to 42°N (except 33°N), with the highest ACCs occurring in the Central CCS, peaking at 0.67 at 35°N. Note also that the MMM skill is as high as or better than the best individual model, which is likely due to greater reliability and the cancellation of individual model errors (Hagedorn et al., 2005).

Probabilistic forecasts of lower tercile STI (i.e., early spring transitions) from CanCM4i and CESM1 are better than random chance from 37°N–40°N (Figure 3a). CanESM5 also shows skill at predicting early spring transitions around 37°N–39°N. Consistent with the ACC results, the MMM probabilistic forecasts are more skillful for larger portions of the CCS than individual models, with BSS > 0 from 37°N–43°N and again at 47°N. Similarly, MMM probabilistic forecasts of upper tercile STI values (i.e., late spring transitions) are also skillful from 31°N–42°N, excluding 34°N (Figure 3b). Recall that the late spring transition forecasts from 31°N–36°N are targeting STI values in a percentile bin that is smaller than the upper 33% typically used for terciles (see Methods).

10.1029/2024GL111083

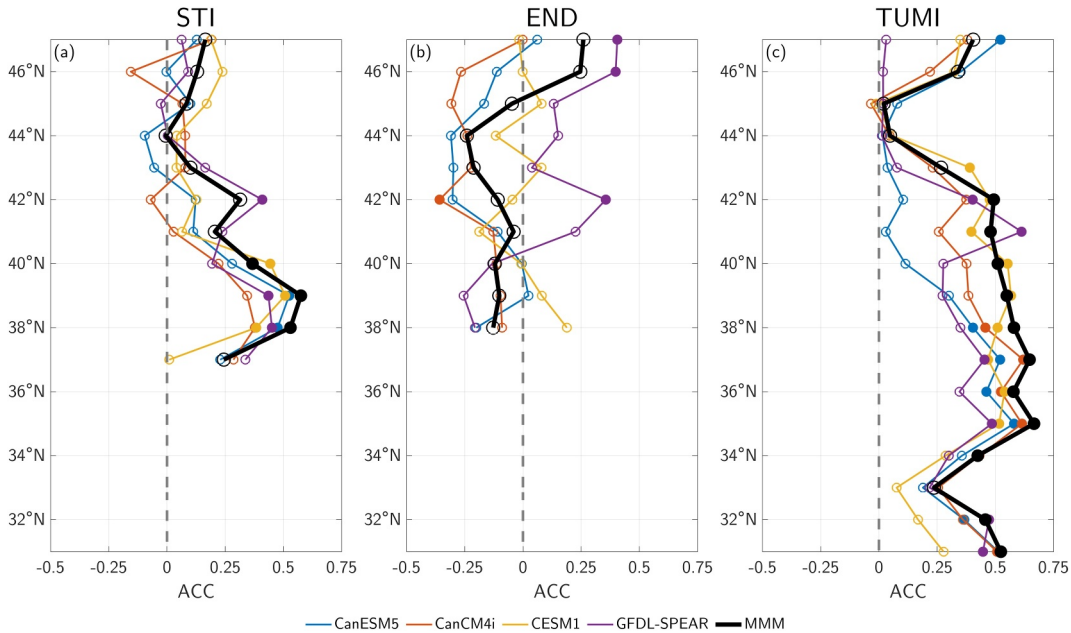

Figure 2. January initialized forecast skill (ACC) of (a) STI, (b) END, and (c) TUMI for each model (colored lines) and the MMM (black lines). Filled circles denote ACC values that are significantly greater than 0 with 95% confidence.

Probabilistic forecasts of END are usually no better than random chance (Figures 3c and 3d). In contrast, all of the models produce probabilistic forecasts of below and above average TUMI that are skillful for large portions of the CCS (Figures 3e and 3f). For example, CanESM5 and CanCM4i produce below average TUMI forecasts with BSS > 0 from 34°N–43°N. The MMM below average TUMI forecast has BSS > 0 at all latitudes except 33°N. Above average TUMI forecasts from 31°N–37°N have BSS > 0 for all models, peaking at BSS = 0.43 at 35°N in the MMM. Above average TUMI forecasts are less skillful from 38°N–47°N, but are generally still better than random chance in the MMM (except at 42°N–44°N).

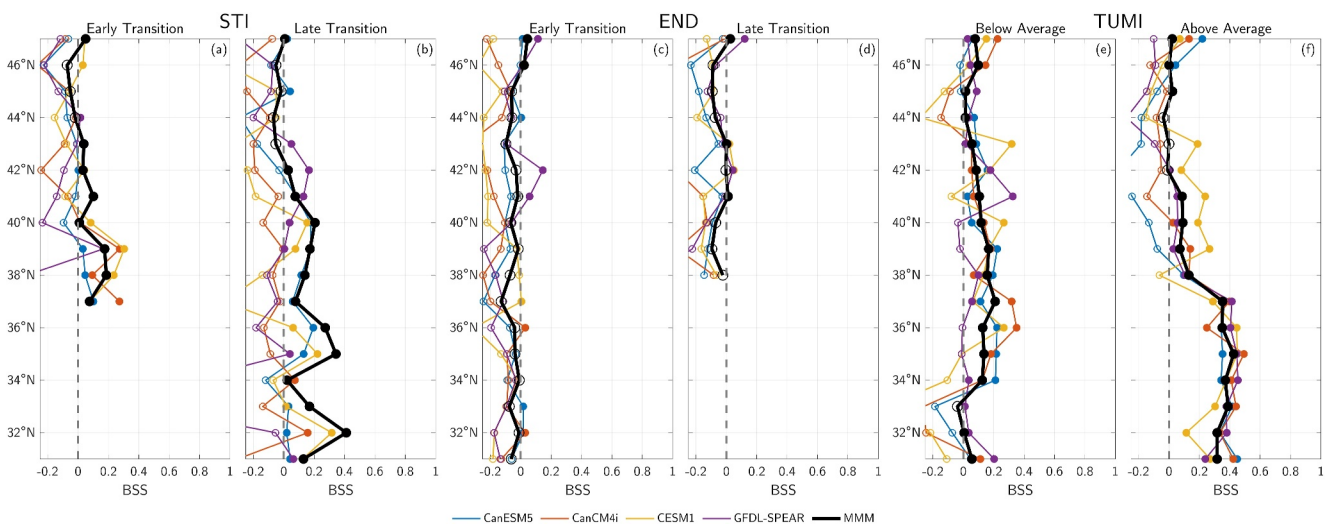

Figure 3. January initialized probabilistic forecast skill (BSS) in upper and lower terciles of (a–b) STI, (c–d) END, and (e–f) TUMI for each model (colored lines) and the MMM (black lines). Forecasts with BSS greater than 0 (filled circles) are better than random chance.

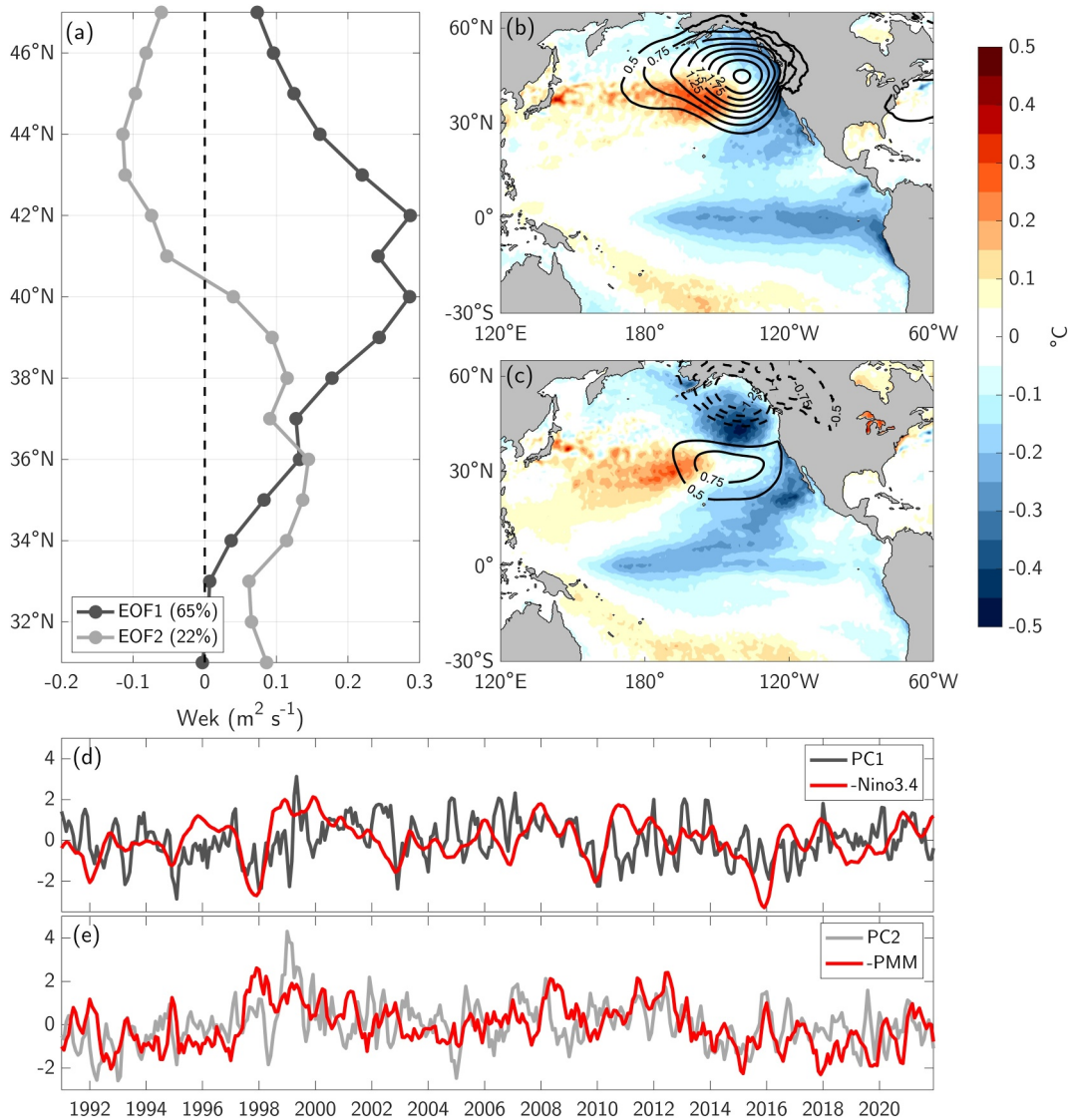

Figure 4. (a) First two EOFs of observed coastal upwelling in the CCS from 1991 to 2021. (b) Regression of observed SSTAs (shading; ˚C) and SLPAs (contours; hPa) onto PC1. (c) As in panel (b), but for PC2. (d) Standardized PC1 (dark gray) with -Nino3.4 (red) overlaid. (e) As in panel (d), but for PC2 and -PMM index. Note that the sign of Nino3.4 and the PMM index have been flipped for comparison with the PCs.

3.3. Sources of Upwelling Predictability

Surface wind stress is strongly impacted by weather noise, which is difficult to predict at lead times beyond ~2 weeks. However, the significant W_{ek} forecast skill on seasonal timescales (Figure 1) suggests that there are deterministic climate processes contributing to W_{ek} predictability. To investigate, we calculate the first two EOFs of observed monthly mean W_{ek} anomalies across all months from 31°N–47°N (Figure 4a). The first EOF explains 65% of the variance and is associated with upwelling anomalies at all latitudes, peaking at 40°N–42°N. The second EOF explains 22% of the variance and depicts a dipole structure, with downwelling (upwelling) anomalies north (south) of 41°N.

Linearly regressing Pacific SSTAs onto the first PC (PC1; Figure 4d) shows a La Niña-like pattern in the tropics, with cool anomalies also present along the North American west coast (Figure 4b). Regressing SLPAs onto PC1 shows a weaker Aleutian Low over the Northeast Pacific, which would produce upwelling-favorable wind anomalies along the U.S. west coast, consistent with the positive W_{ek} anomalies seen in EOF1. The monthly

variance of PC1 peaks in December–February (DJF), indicating that this pattern is most energetic in winter (Figure S5 in Supporting Information S1). Overall, the evidence suggests that EOF1 is related to ENSO's impact on CCS W_{ek} anomalies, consistent with prior analysis of a single model (Jacox et al., 2019). Indeed, the ACC between the DJF averaged PC1 and Nino3.4 index is -0.45 ($p = 0.01$). Therefore, ENSO teleconnections likely provide an important source of W_{ek} forecast skill during wintertime.

Regressing Pacific SSTAs onto PC2 (Figure 4e) reveals a horseshoe pattern of anomalous cooling with minima in the subtropical Northeast Pacific and the Gulf of Alaska, and weaker cooling along the equatorial strip (Figure 4c). The pattern of subtropical cooling is reminiscent of the PMM, a coupled mode of climate variability that often precedes ENSO events (Amaya, 2019; Chiang & Vimont, 2004). This association is further supported by regressions of SLPAs onto PC2, which show negative values over the Gulf of Alaska and positive values over the subtropics. This dipole structure strongly resembles the NPO, a primarily stochastic mode of atmospheric variability that can excite the PMM in boreal winter and spring (Amaya, 2019 and references therein). A positive NPO phase (depicted in Figure 4c) would tend to weaken the climatological North Pacific Subtropical High while simultaneously deepening the Aleutian Low, leading to downwelling-favorable wind anomalies in the North CCS and upwelling-favorable wind anomalies in the Central/South CCS (Di Lorenzo et al., 2008), consistent with EOF2. The monthly variance of PC2 peaks in December-June (Figure S5 in Supporting Information S1), the seasons in which the PMM and NPO tend to be most active (Amaya, 2019). The ACCs between PC2 and seasonally averaged NPO and PMM indices peak at -0.53 ($p = 0.002$) in DJF and -0.52 ($p = 0.003$) in January–March (JFM), respectively.

Further investigation reveals that the PMM index is positively (negatively) correlated with W_{ek} anomalies in the North (South) CCS from about November–February (Figure S6 in Supporting Information S1). However, because the PMM is driven by the NPO during boreal winter, it is likely that a portion of these significant correlations are the result of common forcing, rather than the PMM directly impacting W_{ek} variability. Indeed, we see significant negative correlations between W_{ek} anomalies and the NPO index from 31°N–38°N in January–February (Figure S7 in Supporting Information S1). There are, however, significant negative correlations between the PMM and W_{ek} in the Central CCS from about March–July that may not directly be related to NPO forcing. While the PMM is well-known for its teleconnections to the tropics, it can also influence mid-latitude surface winds via the Summer Deep Convection (SDC) response (Amaya et al., 2019). For example, a negative PMM event (depicted in Figure 4c) would tend to shift the ITCZ southward, leading to reduced off-equatorial convection and anti-cyclonic atmospheric circulation anomalies in the subtropics. These circulation anomalies would then tend to strengthen the North Pacific Subtropical High, driving enhanced alongshore winds and increased upwelling in the South-Central CCS [for a visual representation of the SDC mechanism, see schematic illustrations in Amaya (2019) and Amaya et al. (2019)]. As a result, it is possible that the PMM directly contributes to W_{ek} predictability in the spring/summer.

4. Discussion

We have evaluated the forecast skill of wind-driven upwelling (W_{ek}) in the CCS based on four global climate models contributing to NMME. The model forecasts exhibited significant skill at predicting W_{ek} intensity, particularly from 35°N–47°N when verifying in boreal winter at 0.5–11.5-month lead and from 31°N–40°N when verifying in spring/summer at 0.5–7.5-month lead (Figure 1). The models also skillfully predicted upwelling phenology, including the timing of the spring transition and the total vertical transport integrated over the course of the upwelling season (Figures 3 and 4).

Long-lead skill likely results from large-scale climate modes, which impart deterministic forcing on CCS wind stresses on seasonal timescales and increases their predictability. The importance of ENSO in driving W_{ek} variability in winter (Figure 4) is expected; many previous studies have shown that ENSO is the main source of wintertime predictability in the CCS (e.g., Jacox et al., 2020). However, it is somewhat surprising to discover that the NPO and the PMM may influence W_{ek} predictability in winter-summer. The NPO has historically been considered stochastic, suggesting its timing, intensity, and downstream impacts on surface variables (e.g., CCS wind stress) may be difficult to predict. Although, recent studies suggest that the NPO can be excited by other climate modes, like Central Pacific (CP) ENSO (e.g., Ding et al., 2022), which could give rise to a more deterministic and predictable evolution.

Whether stochastically generated or remotely forced, there is previous evidence that the NPO can directly impact forecast skill in the CCS through its influence on surface winds. In particular, Cluett et al. (2024) showed that CCS SSTA forecasts have less error when the models accurately predict NPO-related atmospheric circulation anomalies 1–2 months prior. Our results combined with these recent studies suggest that the NPO could indeed be a plausible source of W_{ek} forecast skill, especially in boreal winter when it is most energetic. The PMM's possible influence on CCS W_{ek} predictability via the SDC mechanism (Amaya et al., 2019) is intriguing, and supports previous theories for different sources of upwelling variability in winter versus summer (e.g., Black et al., 2011). In particular, Larson and Kirtman (2014) showed that the PMM is predictable up to 6-month in advance. Therefore, the long-lead W_{ek} forecast skill seen in the South-Central CCS during boreal spring/summer could partially result from an accurate PMM forecast during those seasons (Figure 1). Still, more investigation into the physical mechanisms that link the PMM to CCS predictability during the warm season is needed.

Our results build on a growing body of literature highlighting the potential value of seasonal climate forecasts as inputs to decision support tools for marine resource management (Cannizzo & Selz, 2021; Jacox et al., 2020; Tommasi et al., 2017). Indeed, the overall skill of the NMME models in predicting the timing and intensity of the CCS upwelling season is impressive, especially given that these global models were not necessarily optimized to accurately capture the nearshore environment. That said, forecasts could potentially further improve by increasing model spatial resolution to better capture finer scale features known to influence marine ecosystems. Independent of increased resolution, modeling centers could advance the physical representation of upwelling forecasts simply by providing a wider variety of ocean output for analysis. For example, providing daily mean SSH and mixed layer depth forecasts would allow for a more comprehensive evaluation of ocean vertical transport that includes not only the wind-driven component analyzed here, but also the contribution of geostrophic transport to total upwelling (Jacox et al., 2018). Therefore, we echo previous studies (e.g., Jacox et al., 2023; Minobe et al., 2022) calling for the co-development of a broader suite of ecologically relevant ocean forecasts from the current generation of climate models as well as regionally refined simulations for more tailored applications.

Data Availability Statement

NOAA's operational daily mean upwelling: Jacox et al. (2018). NOAA OISSTv2: Huang et al. (2021). ERA5 reanalysis: Hersbach et al. (2020). Wind-driven upwelling forecasts from CanCM4i, CanESM5, CESM1, and GFDL-SPEAR can be found at Amaya (2024).

Acknowledgments
We thank two anonymous reviewers and Nate Mantua for their insightful comments and suggestions that improved the quality of this work. We also thank Bill Merryfield and WooSung Lee for providing access to the daily mean wind stress forecasts from CanESM5 and CanCM4i. We further thank Emily Becker for providing access to the CESM1 wind stress forecasts. This work was supported by the NOAA MAPP program.

References

Amaya, D. (2024). Seasonal upwelling forecasts in the California Current System [Dataset]. *Zenodo*. https://doi.org/10.5281/zenodo.14037267

Amaya, D. J. (2019). The Pacific meridional mode and ENSO: A review. *Current Climate Change Reports*, *5*(4), 296–307. https://doi.org/10.1007/s40641-019-00142-x

Amaya, D. J., Alexander, M. A., Scott, J. D., & Jacox, M. G. (2023). An evaluation of high-resolution ocean reanalyses in the California current system. *Progress in Oceanography*, *210*, 102951. https://doi.org/10.1016/j.pocean.2022.102951

Amaya, D. J., Jacox, M. G., Dias, J., Alexander, M. A., Karnauskas, K. B., Scott, J. D., & Gehne, M. (2022). Subseasonal-to-Seasonal forecast skill in the California Current System and its connection to coastal Kelvin Waves. *Journal of Geophysical Research: Oceans*, *127*(1), e2021JC017892. https://doi.org/10.1029/2021JC017892

Amaya, D. J., Kosaka, Y., Zhou, W., Zhang, Y., Xie, S. P., & Miller, A. J. (2019). The North Pacific pacemaker effect on historical ENSO and its mechanisms. *Journal of Climate*, *32*(22), 7643–7661. https://doi.org/10.1175/JCLI-D-19-0040.1

Barth, J. A., Menge, B. A., Lubchenco, J., Chan, F., Bane, J. M., Kirincich, A. R., et al. (2007). Delayed upwelling alters nearshore coastal ocean ecosystems in the northern California current. *Proceedings of the National Academy of Sciences*, *104*(10), 3719–3724. https://doi.org/10.1073/pnas.0700462104

Becker, E. J., Kirtman, B. P., L'Heureux, M., Muñoz, Á. G., & Pegion, K. (2022). A decade of the North American multimodel ensemble (NMME): Research, application, and future directions. *Bulletin of the American Meteorological Society*, *103*(3), E973–E995. https://doi.org/10.1175/BAMS-D-20-0327.1

Black, B. A., Schroeder, I. D., Sydeman, W. J., Bograd, S. J., Wells, B. K., & Schwing, F. B. (2011). Winter and summer upwelling modes and their biological importance in the California Current Ecosystem. *Global Change Biology*, *17*(8), 2536–2545. https://doi.org/10.1111/j.1365-2486.2011.02422.x

Bograd, S. J., Schroeder, I., Sarkar, N., Qiu, X., Sydeman, W. J., & Schwing, F. B. (2009). Phenology of coastal upwelling in the California Current. *Geophysical Research Letters*, *36*(1), L01602. https://doi.org/10.1029/2008GL035933

Cannizzo, Z. J., & Selz, V. (2021). National marine sanctuary climate change science priorities workshop report. https://doi.org/10.25923/4FTJ-3F44

Capet, X. J., Marchesiello, P., & McWilliams, J. C. (2004). Upwelling response to coastal wind profiles. *Geophysical Research Letters*, *31*(13), L13311. https://doi.org/10.1029/2004GL020123

Chavez, F. P., & Messié, M. (2009). A comparison of eastern boundary upwelling ecosystems. *Progress in Oceanography*, *83*(1–4), 80–96. https://doi.org/10.1016/j.pocean.2009.07.032

Chiang, J. C. H., & Vimont, D. J. (2004). Analogous Pacific and Atlantic meridional modes of tropical atmosphere-ocean variability. *Journal of Climate*, *17*(21), 4143–4158. https://doi.org/10.1175/JCLI4953.1

Cluett, A. A., Jacox, M. G., Amaya, D. J., Alexander, M. A., & Scott, J. D. (2024). Atmospheric precursors of skillful SST prediction in the Northeast Pacific. *Journal of Climate*, *37*(20), 5337–5353. https://doi.org/10.1175/JCLI-D-24-0121.1

Delworth, T. L., Cooke, W. F., Adcroft, A., Bushuk, M., Chen, J.-H., Dunne, K. A., et al. (2020). SPEAR: The next generation GFDL modeling system for seasonal to multidecadal prediction and projection. *Journal of Advances in Modeling Earth Systems*, *12*(3), e2019MS001895. https://doi.org/10.1029/2019MS001895

Di Lorenzo, E., Schneider, N., Cobb, K. M., Franks, P. J. S., Chhak, K., Miller, A. J., et al. (2008). North Pacific Gyre Oscillation links ocean climate and ecosystem change. *Geophysical Research Letters*, *35*(8), L08607. https://doi.org/10.1029/2007GL032838

Ding, H., Alexander, M. A., & Jacox, M. G. (2021). Role of geostrophic currents in future changes of coastal upwelling in the California Current System. *Geophysical Research Letters*, *48*(3), e2020GL090768. https://doi.org/10.1029/2020gl090768

Ding, R., Tseng, Y.-H., Di Lorenzo, E., Shi, L., Li, J., Yu, J.-Y., et al. (2022). Multi-year El Niño events tied to the North Pacific oscillation. *Nature Communications*, *13*(1), 3871. https://doi.org/10.1038/s41467-022-31516-9

Diro, G. T., Merryfield, W. J., Lin, H., Lee, W.-S., Muncaster, R., Kharin, V. V., et al. (2024). *The Canadian seasonal to interannual prediction system version 3.0 (CanSIPSv3.0). Technical Report*. (pp. 1–51). Environment and Climate Change Canada. Retrieved from https://collaboration.cmc.ec.gc.ca/cmc/cmoi/product_guide/docs/tech_notes/technote_cansips-300_e.pdf

Hagedorn, R., Doblas-Reyes, F. J., & Palmer, T. N. (2005). The rationale behind the success of multi-model ensembles in seasonal forecasting — I. Basic concept. *Tellus A: Dynamic Meteorology and Oceanography*, *57*(3), 219–233. https://doi.org/10.3402/tellusa.v57i3.14657

Henson, S. A., & Thomas, A. C. (2007). Interannual variability in timing of bloom initiation in the California Current System. *Journal of Geophysical Research*, *112*(C8), C08007. https://doi.org/10.1029/2006JC003960

Hersbach, H., Bell, B., Berrisford, P., Hirahara, S., Horányi, A., Muñoz-Sabater, J., et al. (2020). The ERA5 global reanalysis. *Quarterly Journal of the Royal Meteorological Society*, *146*(730), 1999–2049. https://doi.org/10.1002/qj.3803

Hervieux, G., Alexander, M. A., Stock, C. A., Jacox, M. G., Pegion, K., Becker, E., et al. (2019). More reliable coastal SST forecasts from the North American multimodel ensemble. *Climate Dynamics*, *53*(12), 7153–7168. https://doi.org/10.1007/s00382-017-3652-7

Hobday, A. J., Spillman, C. M., Eveson, J. P., Hartog, J. R., Zhang, X., & Brodie, S. (2018). A framework for combining seasonal forecasts and climate projections to aid risk management for fisheries and aquaculture. *Frontiers in Marine Science*, *5*(APR), 331717. https://doi.org/10.3389/fmars.2018.00137

Huang, B., Liu, C., Banzon, V., Freeman, E., Graham, G., Hankins, B., et al. (2021). Improvements of the daily optimum interpolation sea surface temperature (DOISST) version 2.1. *Journal of Climate*, *34*(8), 2923–2939. https://doi.org/10.1175/JCLI-D-20-0166.1

Jacox, M. G., Alexander, M. A., Amaya, D., Becker, E., Bograd, S. J., Brodie, S., et al. (2022). Global seasonal forecasts of marine heatwaves. *Nature*, *604*(7906), 486–490. https://doi.org/10.1038/s41586-022-04573-9

Jacox, M. G., Alexander, M. A., Siedlecki, S., Chen, K., Kwon, Y. O., Brodie, S., et al. (2020). Seasonal-to-interannual prediction of North American coastal marine ecosystems: Forecast methods, mechanisms of predictability, and priority developments. *Progress in Oceanography*, *183*, 102307. https://doi.org/10.1016/j.pocean.2020.102307

Jacox, M. G., Alexander, M. A., Stock, C. A., & Hervieux, G. (2019). On the skill of seasonal sea surface temperature forecasts in the California Current System and its connection to ENSO variability. *Climate Dynamics*, *53*(12), 7519–7533. https://doi.org/10.1007/s00382-017-3608-y

Jacox, M. G., Buil, M. P., Brodie, S., Alexander, M. A., Amaya, D. J., Bograd, S. J., et al. (2023). Downscaled seasonal forecasts for the California Current System: Skill assessment and prospects for living marine resource applications. *PLOS Climate*, *2*(10), e0000245. https://doi.org/10.1371/journal.pclm.0000245

Jacox, M. G., Edwards, C. A., Hazen, E. L., & Bograd, S. J. (2018). Coastal upwelling revisited: Ekman, Bakun, and improved upwelling indices for the U.S. West coast. *Journal of Geophysical Research: Oceans*, *123*(10), 7332–7350. https://doi.org/10.1029/2018JC014187

Jorgensen, E. M., Hazen, E. L., Jacox, M. G., Pozo Buil, M., Schroeder, I., & Bograd, S. J. (2024). Physical and biogeochemical phenology of coastal upwelling in the California current system. *Geophysical Research Letters*, *51*(7), e2024GL108194. https://doi.org/10.1029/2024GL108194

Kearney, K. A., Alexander, M., Aydin, K., Cheng, W., Hermann, A. J., Hervieux, G., & Ortiz, I. (2021). Seasonal predictability of sea ice and bottom temperature across the eastern Bering Sea Shelf. *Journal of Geophysical Research: Oceans*, *126*(11), e2021JC017545. https://doi.org/10.1029/2021JC017545

Kirtman, B. P., Min, D., Infanti, J. M., Kinter, J. L., Paolino, D. A., Zhang, Q., et al. (2014). The North American multimodel ensemble: Phase-1 seasonal-to-interannual prediction; phase-2 toward developing intraseasonal prediction. *Bulletin of the American Meteorological Society*, *95*(4), 585–601. https://doi.org/10.1175/BAMS-D-12-00050.1

Larson, S. M., & Kirtman, B. P. (2014). The pacific meridional mode as an ENSO precursor and predictor in the North American multimodel ensemble. *Journal of Climate*, *27*(18), 7018–7032. https://doi.org/10.1175/JCLI-D-14-00055.1

Lin, H., Merryfield, W. J., Muncaster, R., Smith, G. C., Markovic, M., Dupont, F., et al. (2020). The Canadian seasonal to interannual prediction system version 2 (CanSIPSv2). *Weather and Forecasting*, *35*(4), 1317–1343. https://doi.org/10.1175/WAF-D-19-0259.1

Lu, F., Harrison, M. J., Rosati, A., Delworth, T. L., Yang, X., Cooke, W. F., et al. (2020). GFDL's SPEAR seasonal prediction system: Initialization and ocean tendency adjustment (OTA) for coupled model predictions. *Journal of Advances in Modeling Earth Systems*, *12*(12), e2020MS002149. https://doi.org/10.1029/2020MS002149

Minobe, S., Capotondi, A., Jacox, M. G., Nonaka, M., & Rykaczewski, R. R. (2022). Toward regional marine ecological forecasting using global climate model predictions from subseasonal to decadal timescales: Bottlenecks and recommendations. *Frontiers in Marine Science*, *9*, 855965. https://doi.org/10.3389/fmars.2022.855965

Neveu, E., Moore, A. M., Edwards, C. A., Fiechter, J., Drake, P., Crawford, W. J., et al. (2016). An historical analysis of the California Current circulation using ROMS 4D-Var: System configuration and diagnostics. *Ocean Modelling*, *99*, 133–151. https://doi.org/10.1016/j.ocemod.2015.11.012

Payne, M. R., Hobday, A. J., MacKenzie, B. R., Tommasi, D., Dempsey, D. P., Fässler, S. M. M., et al. (2017). Lessons from the first generation of marine ecological forecast products. *Frontiers in Marine Science*, *4*(SEP), 289. https://doi.org/10.3389/fmars.2017.00289

Schwing, F. B., Bond, N. A., Bograd, S. J., Mitchell, T., Alexander, M. A., & Mantua, N. (2006). Delayed coastal upwelling along the U.S. West coast in 2005: A historical perspective. *Geophysical Research Letters*, *33*(22), L22S01. https://doi.org/10.1029/2006GL026911

Siedlecki, S. A., Kaplan, I. C., Hermann, A. J., Nguyen, T. T., Bond, N. A., Newton, J. A., et al. (2016). Experiments with Seasonal Forecasts of ocean conditions for the Northern region of the California Current upwelling system. *Scientific Reports*, *6*(1), 27203. https://doi.org/10.1038/srep27203

Small, R. J., Bacmeister, J., Bailey, D., Baker, A., Bishop, S., Bryan, F., et al. (2014). A new synoptic scale resolving global climate simulation using the Community Earth System Model. *Journal of Advances in Modeling Earth Systems*, *6*(4), 1065–1094. https://doi.org/10.1002/2014MS000363

Sospedra-Alfonso, R., Merryfield, W. J., Boer, G. J., Kharin, V. V., Lee, W.-S., Seiler, C., & Christian, J. R. (2021). Decadal climate predictions with the Canadian Earth system model version 5 (CanESM5). *Geoscientific Model Development*, *14*(11), 6863–6891. https://doi.org/10.5194/gmd-14-6863-2021

Stock, C. A., Pegion, K., Vecchi, G. A., Alexander, M. A., Tommasi, D., Bond, N. A., et al. (2015). Seasonal sea surface temperature anomaly prediction for coastal ecosystems. *Progress in Oceanography*, *137*, 219–236. https://doi.org/10.1016/j.pocean.2015.06.007

Tommasi, D., Stock, C. A., Hobday, A. J., Methot, R., Kaplan, I. C., Eveson, J. P., et al. (2017). Managing living marine resources in a dynamic environment: The role of seasonal to decadal climate forecasts. *Progress in Oceanography*, *152*, 15–49. https://doi.org/10.1016/j.pocean.2016.12.011